J Mater Sci (2007) 42:2899–2902
DOI 10.1007/s10853-006-0669-4

LETTER

On the intergranular embrittlement of a solid-solution strengthened Fe-base alloy by internal oxidation

H. M. Tawancy

Received: 12 June 2006 / Accepted: 13 July 2006 / Published online: 15 March 2007

High-temperature structural applications of solid-solution strengthened superalloys is largely based upon their potentially useful combination of properties particularly mechanical strength, environmental resistance, and ease of fabrications, e.g. [1]. Typically, these alloys are supplied by the manufacturers in the solution-annealed condition with a given set of properties corresponding to characteristic microstructural features. Subsequent fabrication processes, however, can significantly alter the initial microstructure and properties. Therefore, an important consideration should be given to these effects in alloy selection as well as in assessing material performance. Also, the interaction between mechanical and chemical properties in certain environments should be taken into account.

For many furnace applications in the petrochemical industry, high-temperature alloys are used in the form of tubes where the desired length is produced by welding of individual sections. In such applications, thermal and environment-induced embrittlement is of major concern. It is the objective of this study to demonstrate the effect of as-welded structures on the relationship between mechanical strength and oxidation resistance of an Fe-32Ni–22Cr–0.80 Mn–0.46Al–0.37Si–0.08C alloy (all in weight %) under actual service conditions. Welded tubes (internal diameter = 0.11 m, wall thickness = 0.014 m) in the same condition to be used in practice were installed in a benzene plant and exposed to an environment consisting of 64.3% H_2-18.92%C_1-3.48C_2-0.96C_3-0.03C_4-0.24C_5-1.5%C_6-C_8 NON-ARO, 5.91% benzene-1.45% C_8 aromatics-0.04%C_9-0.15% diphenyl at 600 °C. Light optical metallography and scanning electron microscopy were used to characterize the microstructure.

During the field test, the maximum principal stress developed in the tube was less than one-half the respective yield strength of the material. However, after about 1,000 h, the tube was fractured in the weld heat-affected zone. All micrographs presented below were derived from cross-sections of the tube near the internal surface. Grain structures representative of the base metal and weld-heat affected zone near the major fracture are shown in the backscattered electron images of Fig. 1. As can be seen, the weld heat-affected zone had coarser grains relative to the base metal. Also, the average microhardness of the weld heat-affected zone was HV 268 (R_c 25) as compared to HV 224 (R_b 95) corresponding to the base metal. Since no secondary precipitates could be detected down to the scale of transmission electron microscopy, it was concluded that the observed difference in hardness could be related to residual stresses within the heat-affected zone. Examination of the fracture surface revealed that the fracture mode was intergranular as shown in Fig. 2a. However, at higher magnifications, dimples characteristic of microvoid coalescence were observed at separated grain facets as demonstrated in Fig. 2b. These characteristics are typical of ductile intergranular fracture where the deformation preceding fracture is

H. M. Tawancy (✉)
Materials Characterization Laboratory, Center for Engineering Research, Research Institute, King Fahd University of Petroleum and Minerals, P.O. Box 1639, Dhahran 31261, Saudi Arabia
e-mail: tawancy@kfupm.edu.sa

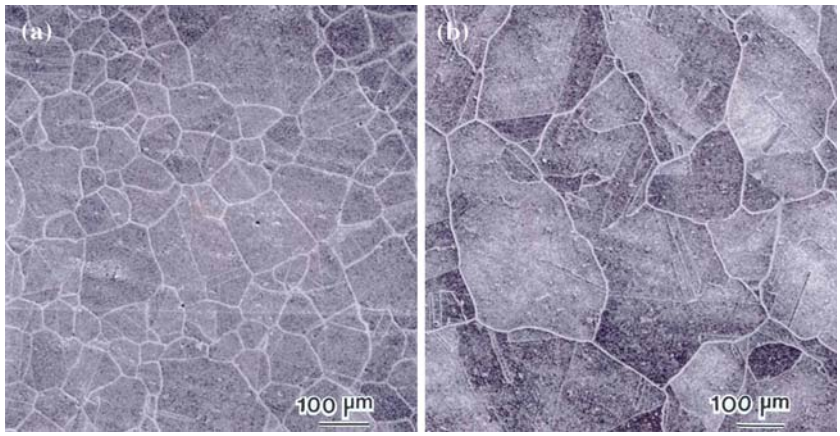

Fig. 1 Backscattered electron images showing typical grain structures. (**a**) Base metal, (**b**) Weld heat-affected zone

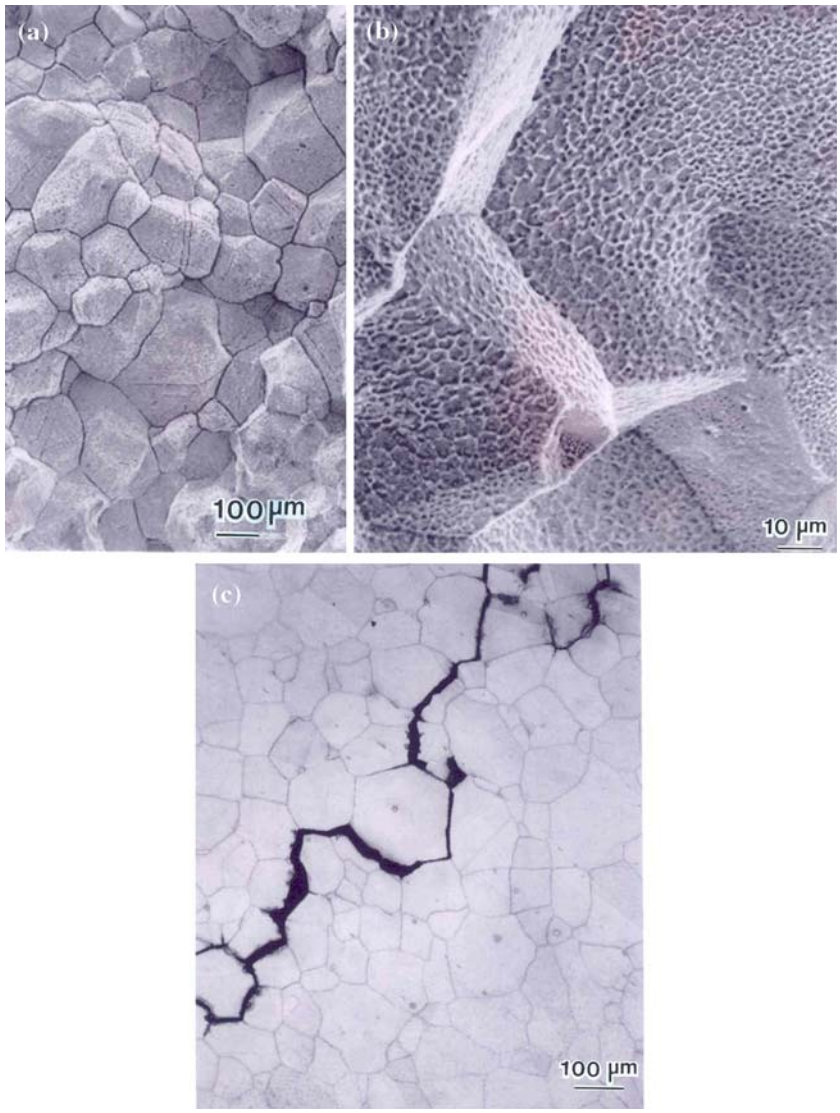

Fig. 2 Characteristic features of the fracture mode. (**a**) Secondary electron image of the fracture surface showing an intergranular mode, (**b**) Secondary electron image showing dimples at separated grain facets, (**c**) Light optical micrograph showing secondary cracks along grain boundaries

localized alongside grain boundaries as a result of alloy-depleted zones [2]. Secondary intergranular cracks are shown in Fig. 2c.

Detailed examination of the grain boundaries revealed the presence of a network of secondary phase(s) as illustrated in the example of Fig. 3. In the

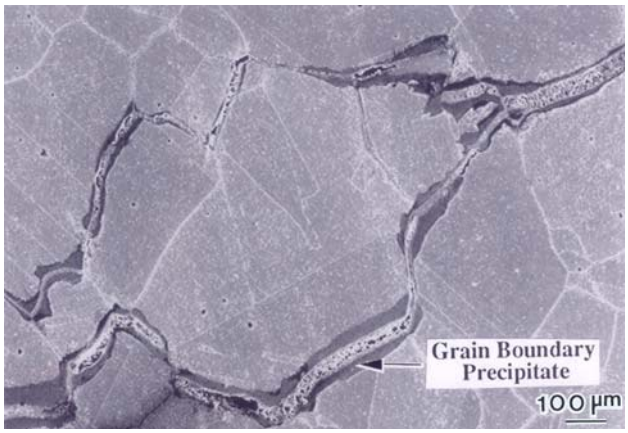

Fig. 3 Backscattered electro image illustrating a continuous layer of grain boundary precipitate

backscattered imaging mode, three phases could be distinguished as shown in Fig. 4a. Corresponding X-ray spectra illustrating the elemental compositions of the regions marked 1, 2, and 3 in (a) are shown in (b), (c), and (d) respectively. Figure 4e summarizes the results of quantifying the spectral data. It is evident that the phase closest to the grain boundary (region 3) consisted of a Ni-rich solid-solution. The adjacent region marked 2 appeared to consist of an oxide based upon the composition $(Cr,Fe)_2O_3$. Although region 1 also consisted of an oxide likely to be of the type $(Cr,Fe)_2O_3$, however, it was enriched in Cr as compared to the oxide corresponding to region 2. In general, no measurable oxide scale could be detected at the surface. Distinction among the three grain boundary phases is further demonstrated by the X-ray mapping images of Fig. 5 showing the distribution of various elements.

At least three parameters could have contributed to the observed internal oxidation described above. First, various studies have shown that internal oxidation along the grain boundaries is favored by a relatively large grain size, e.g. [3, 4]. Second, at the relatively low temperature employed in this study, the oxidation reaction is likely to be dominated by short-circuit diffusion of oxygen along grain boundaries. Also, this could be promoted by the relatively high localized stresses within the heat-affected zone fusion [5]. Third, under reducing environmental conditions characterized by low oxygen potential, more stable oxides such as Cr_2O_3 could form, however, the formation of less stable Ni-rich oxides would be precluded. In the present case, various concentrations of Fe could replace for Cr leading to the formation of $(Cr,Fe)_2O_3$-type oxides as observed. It is expected that localized deformation leading to intergranular fracture would be concentrated within the relatively soft Ni-rich solid-solution adjacent to grain boundaries leading to the observed fracture characteristics. The reaction leading to intergranular oxidation could then be expressed as:

Grain boundary zone (Fe,Cr,Ni) + Oxygen → (Cr,Fe) oxides + Ni-rich solid-solution indicating that although the environment was reducing to Ni–NiO, it was oxidizing to both Cr–Cr_2O_3 and Fe–Fe_2O_3. This type of grain boundary oxidation usually involves

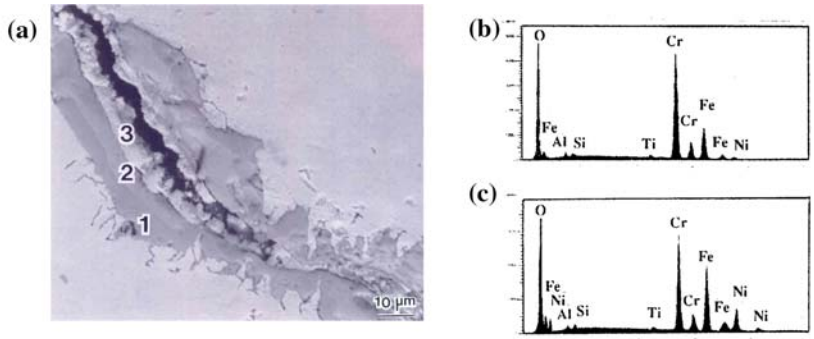

(e) **Chemical Compositions (Atomic %)**

Element	Region 1	Region 2	Region 3
Cr	20.6	15.2	2.4
Fe	9.0	14.7	25.3
Ni	0.7	7.1	72.3
Al	0.9	0.7	-
Ti	0.3	0.3	-
Si	0.6	0.6	-
O	67.9	61.4	-

Fig. 4 Analysis of grain boundary precipitates. (**a**) Backscattered electron image. (**b**), (**c**), and (**d**) Energy dispersive X-ray spectra derived from the regions marked 1, 2, and 3 in (**a**) respectively. (**e**) Results of quantifying the spectral data

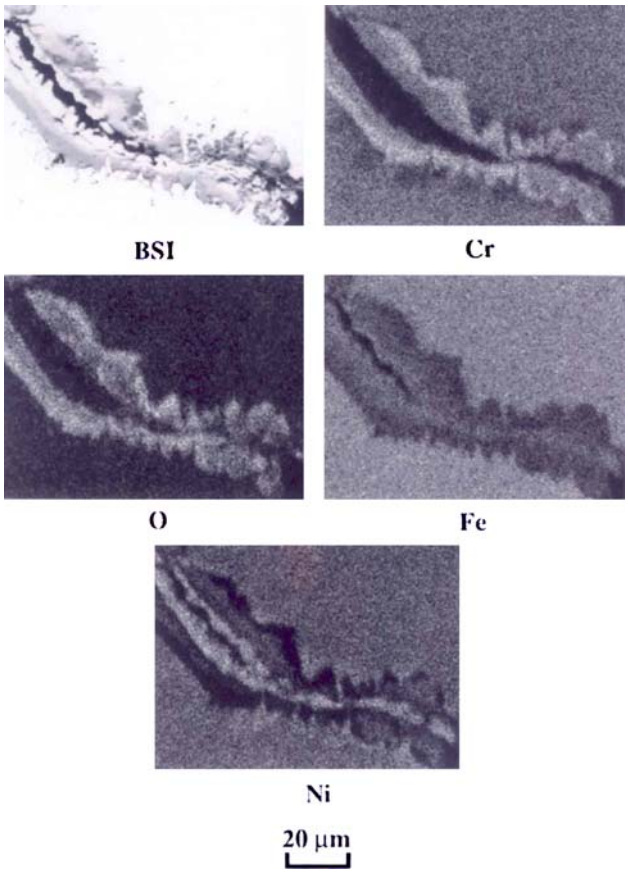

Fig. 5 Backscattered electron image and corresponding X-ray mapping images illustrating the distribution of Cr, O, Fe, and Ni within the grain boundary phases

oxidation following carburization as reported in an earlier study [6].

Acknowledgement The support of the Research Institute of King Fahd University of Petroleum and Mineral is greatly appreciated.

References

1. Tawancy HM (1994) Structure and properties of high-temperature alloys. KFUPM Press, Dhahran, p 11
2. Metals Handbook (1974) Fractography and atlas of fractographs. vol. 9, 8th edition ASM, Metals Park, Ohio, p 112
3. Rothman MF, Storey IJ (2005) Reliability and longevity of furnace components as influenced by alloy construction. HAYNES International Publication No. H-3124A, Kokomo, Indiana
4. Pettit FS, Giggins CS, Goebel JA, Felton EJ (1976) In: Tien JK, Ansell GS (eds) Alloy and microstructural design. Academic Press, New York, p 375
5. Krupp U, Kane W, Pfacendtner JA, Liu X, Laird C, Laird C, McMahon CJ Jr (2004) Mater Res 7:35
6. Meier AGH, Perkins RA, Coons WC (1982) Oxid Met 17:235